A comparison between the microstructure and the functional properties of NiW coatings produced by magnetron sputtering and electrodeposition

Dewis Figuel, Alain Billard, Catherine Savall, Juan Creus, Stéphane Cohendoz, Jean-Luc Grosseau-Poussard

A comparison between the microstructure and the functional properties of NiW coatings produced by magnetron sputtering and electrodeposition

D. Figuet [a], A. Billard b, C. Savall [a], J. Creus [a], S. Cohendoz [a], J.L. Grosseau-Poussard [a,*]

a Laboratoire des Sciences de l'Ing´enieur pour l'Environnement (LaSIE), Universit´e de La Rochelle, CNRS UMR 7356, Avenue Michel Cr´epeau, 17042, La Rochelle Cedex 1, France

b FEMTO-ST Institute (UMR CNRS 6174), Universit´e Bourgogne Franche-Comt´e, UTBM, 2 Place Lucien Tharradin, F-25200 Montb´eliard Cedex, France

Abstract :
The functional properties of both electrodeposited and sputtered nickel and NiW nanostructured alloys are discussed as a function of their main microstructural features. As W is incorporated into the Ni matrix, several metallurgical parameters that can influence the functional properties were also modified, namely grain size, crystallographic texture, morphology and element contamination. The hardness measurements for the different coatings were analysed in terms of both grain size and W incorporation effects. In addition, the high level of Argon, particularly for the NiW-PVD coating, was shown to be responsible for the highest hardness value ob-tained. Comparing the behavior of NiW coatings with that of pure nickel in both elaboration processes shows that tungsten incorporation greatly enhances abrasion resistance.

Keyword : Ni–W, Sputtering , Electrodeposition, Nanocrystalline alloys Hardness and modulus Adhesion and abrasion resistance Microstructure

Introduction:

In industrial fields such as aeronautics, automotive industry, nuclear energy and electronics, materials are subjected to severe mechanical and environmental stress. So, durability is a significant issue for structural materials. In order to satisfy these requirements, surface treatment, in particular metallic coatings, are widely used. This is the case for the development of nanomaterials, which have been the subject of numerous studies due to their excellent physicochemical properties. In this context, nickel alloys have been thoroughly investigated for the synergy between their mechanical and chemical properties [1–3]; and for nanocrystalline alloys, NiW coatings have very attractive properties that make them more resistant to both corrosion and wear [4]. This places them among the potential candidates to replace the hard impacted by the REACH regulation [5,6].

The incorporation of an alloying element in a nanocrystalline metallic matrix has been studied in depth and is well documented [7–9]. Its use allows some of the main features of the metallurgical states to be varied, such as grain size, texture index, the nature of the grain boundaries, etc. Furthermore, the addition of an alloying element may lead to a stabilization of the nanostructure at high temperature or during sliding. For example, electrodeposited NiW alloys have nanocrystalline grain structures that do not considerably coarsen when heated to tem-peratures of up to 500 ◦C [10,11]. In addition, in the work of Detor [12] and Quiroga [13], a correlation between grain size and W content was clearly established. This can be explained by a preferential segregation of W at the grain boundaries at low W content,

which induces an enhanced grain boundary contribution. High W incorporation promotes nucleation and at the same time limits grain growth.

NiW coatings are usually obtained by electrodeposition (ED) and numerous studies have been made of their mechanical, tribological and electrochemical behaviour [14–16]. Electrodeposition is an efficient and relatively inexpensive method to produce NiW coatings. Nevertheless, it also presents some disadvantages, including the use of several chemicals with a harmful environmental impact. This process also requires a conductive substrate, and to obtain a crystalline alloy the tungsten composition range that can be obtained by electroplating is limited to 20 at.% W [17].

However, thinking of other applications like micro and nano electro- mechanical systems (MEMS, NEMS), techniques such as physical vapor deposition may be viable alternatives for the deposition of a NiW thin film [18,19]. Very few studies have used physical vapor deposition (PVD) like magnetron sputtering to obtain these deposits [20,21]. Although the process requires more sophisticated and expensive equipment, it can easily be used to vary the tungsten content in an alloy by up to 100 at.%. In addition, it may be used with any kind of substrate, doesn't need specific surface preparation, and the environmental issues are reduced compared to the ED process. The deposition rates are very low compared to the electrodeposition process, which considerably limits the coating thickness, but with this deposition technique we can obtain a uniform composition and thickness for noncomplex sample geometry.

Depending on the elaboration process, the growth and grain nucle-ation mechanisms are not the same. These two phenomena are often in competition, they have an essential influence on the kinetics of coating formation and will also determine the structure and properties of the coating. For ED, the main influence is on parameters such as bath formulation (complexing agents or additives) and the deposition con-ditions (e.g. temperature, electrical parameters) [22,23]. While for PVD, the most influential parameters are the pressure in the deposition chamber, sputtering rate, the distance between the target and the specimen, and the possible presence of reactive species in the chamber. These parameters will influence both the sputtering and redeposition conditions through the mean-free path and the deposited energy per atom [24,25]. For both processes, depending on these different condi-tions and parameters, the resulting microstructures and metallurgical states may vary, and in turn change the functional properties.

As very few studies have been devoted to relatively thin NiW coat-ings (thickness up to 10 µm) obtained either by electrodeposition or sputtering techniques, the aim of the present work was to systematically compare the main microstructural features (e.g. grain size, texture, morphology, roughness, contamination) and their influence on func-tional properties. Thus, films of 10 µm thickness were produced and an identical composition of the alloy was chosen for both processes; a W concentration of 15 at.% was used. This should lead to a nanocrystalline material with a grain size range which is within the limit of the domain where the Hall-Petch law holds, and for which grain boundary processes start to be involved in both the deformation and wear mechanisms. However, the mechanical characteristics should be high at this Wconcentration, and the effect on certain functional properties like adhesion and/or abrasion resistance should be significant. Thus, scratch and wear resistance were also systematically investigated and compared for the processes. In addition, a pure nickel reference material was produced by both PVD and ED for comparison with the NiW alloys.

2. Experimental aspects

2.1. Deposition processes

Concerning the PVD process, the Ni and NiW coatings were depos-ited on steel substrates (35 NiCrMo16; H = 4.0 GPa and E = 200 GPa) with pure Ni and W metallic targets (99.9%) using a DC magnetron sputtering device (Alcatel 450). The targets (145 mm in diameter) were off center from the substrate holder axis. The substrates were located at 115 mm from the axis of the rotating substrate holder, and separated by about 70 mm from the targets. In such conditions, the coatings thickness is uniform (variation less than 5%). The substrates were mechanically ground with SiC paper to grade 4000 then ultrasonically cleaned in ethanol. Before the deposition stage, an in-situ argon ion etching of the substrates was performed. The deposition chamber was pumped down to 10 4 Pa; argon was then introduced for the deposition step at a working pressure of 0.5 Pa. The Ni and W metallic targets were monitored by two power supplies which were used to control the W concentration. The Ni discharge power was set at 265W (1A) and the W discharge power was varied between 0 and about 97 W for tungsten content from 0 to 15 at.%. To reach 10 µm, the deposition lasted a little less than 6 h.

For the electrodeposition process, Ni and NiW were deposited on identical steel substrates in a standard three electrode cell using a VSP potentiostat from Biologic. The anode was a platinum grid for NiW de-posits and a nickel slab for Ni deposits, with a large geometrical surface area compared to that of the working electrode. The surface of the latter varied from 1 to 7 cm2, and had no influence on the characteristic of the coatings. Both coatings were deposited under direct current (DC) with a cathodic current density of 50 mA/cm2. NiW alloys were obtained from an additive free citrate ammonium bath, as initially proposed by Yamasaki et al. [26], containing sodium citrate (Na3C6H5O7·2H2O, 0.5 M), ammonium chloride (NH4Cl, 0.5 M), nickel sulphate ($NiSO_4 \cdot 6H_2O$, 0.06 M), sodium bromide (NaBr, 0.15 M) and sodium tungstate (Na2WO4·2H2O, 0.14 M) at a pH of 9.2. The temperature of the bath was kept at 65 ◦C for the NiW alloy deposits. Ni coatings were deposited from a sulfamate solution containing nickel chloride ($NiCl_2 \cdot 6H_2O$, 0.12 M), nickel sulfamate ($Ni(SO_3NH_2)2 \cdot 4H_2O$, 0.93 M) and boric acid (H_3BO_3, 0.485 M). A balance of nickel carbonate ($NiCO_3.2Ni(OH)_2 \cdot 6H_2O$) was used to adjust the pH to 4.3. For these deposits, the temperature was kept constant at 50 ◦C. This is a standard sulfamate solution for most Ni plating applications for which good corrosion behaviour is also required. ACS reagent grade chemicals and ultra-pure water (18.2 M) were used to prepare the electroplating baths in order to minimize sources of contamination. In each case, the desired thickness is governed by Far-aday's law and is thus dependent on deposit time. So, NiW coatings were deposited for 30 min and Ni coatings for 11 min to target a thickness of 10 µm.

2.2. Characterization

A multiscale approach was undertaken to investigate the micro-structure of the coatings. The crystalline structure was determined using X-ray diffraction (XRD) in θ-2θ mode with a Bruker AXS D8-Advanced diffractometer operating at 40 kV and 40 mA and with Cu-Kα radia-tion. The detector was scanned at 0.01◦ steps and the acquisition time was 0.1 s. The scans were collected with 2θ varying from 40◦ to 105◦. Background noise and the Kα2 radiation ray were stripped by the enhanced Rachinger method with Diffrac. eva software. The experi-mental spectra of a standard Ni sample, with a grain size of 168 µm, was analysed in order to evaluate peak width, similar to instrumental broadening. This latter was subtracted from the

(111) peak width. Finally, the Scherrer equation was used on the (111) peak with the objective of gauging grain size.

The chemical composition of the coatings was obtained by μ-X-ray fluorescence spectroscopy using a Bruker M4 Tornado operating at 35 kV and 300 μA with a Rhodium filament source. Atomic force micro-scopy (AFM) was used to evaluate surface morphology and roughness. AFM images were acquired in contact mode with an Agilent 5500 apparatus. Hot extraction analyses were carried out to evaluate the contamination by non-metallic species using an EMGA-621W oxygen/ nitrogen/hydrogen analyser and an EMIA-920V2 carbon/sulphur ana-lyser from Horiba.

2.3. Evaluation of the mechanical properties

Micro-indentation equipment (Anton Paar MCT3 STEP 4) equipped with a diamond Vickers indenter was used to evaluate the mechanical properties of the coatings. In order to minimize the substrate effect and ensure the reliability of the data, a value less than 1 μm (less than 10% of the coating thickness) was chosen as the penetration depth, whilst 12 microindentations were conducted on each coating. After the tests, the average hardness and elastic modulus values and the standard deviation were calculated using the Oliver and Pharr method [27].

The adhesive strength and abrasion resistance of the coatings were evaluated using a micro-scratch test (Anton Paar MCT3 STEP 4) with a diamond tip (R = 0.1 mm and tape angle 120◦). Scratch tests were performed using a linearly increasing normal load. The maximum load, loading rate and scratch distance were set at 30 N, 60 N/min and 4 mm, respectively. During the scratch test, the coefficient of friction was also simultaneously recorded. The scratched surfaces were analysed by SEM both in surface and cross section views with a FEI Phillips FEG/ESEM quanta 200 operating at 20 kV. After the tests, critical loads could bedetermined from the morphology of the scratches observed by an optical microscope (LEICA CTR6000) and from depth profiles and friction force measurements.

Sliding wear studies were carried out in laboratory air (relative hu-midity of about 60–70%) at room temperature (about 25 ◦C) in unlu-bricated conditions using a pin-on-disc sliding wear tester (TRB3) supplied by Anton Paar. These tests were performed at a constant load of 1 N with a constant linear sliding speed of 15 cm/s. The friction force between the coated substrate and the pin was measured using a trans-ducer and data acquisition was performed at regular intervals. A typical standard 100Cr6 with a 6 mm diameter was used as a spherical coun-terpart. It was the most useful as a bearing ring for tribological appli-cations because of its good wear resistance [28].

After the friction tests in air, the tribo-oxidation products formed at the surface of the specimens were analysed by micro-Raman spectrom-etry with a Jobin Yvon Horiba LabRam HR equipped with a mono-chromatic HeNe laser at a 633 nm wavelength. An optical microscope (LEICA) was also used to evaluate the surface degradation of the coatings.

3. Results and discussion

Pure nickel and NiW alloy coatings were deposited either by ED or PVD, and were called Ni-ED, Ni-PVD, NiW-ED and NiW-PVD, respec-tively. In this section, the main metallurgical features of the coatings are presented. The hardness and Young's Modulus values obtained from the instrumented indentation measurements are also given. The results from scratch

resistance tests are then analysed based on surface and cross- section observations. Finally, the tribological behaviour in air will be discussed.

3.1. Microstructure, phase composition, hardness and Young's modulus

Several characterization methods were used to investigate the metallurgical state and Table 1 presents their main features. X ray fluorescence showed that the W concentration was about 15 at. % for both ED and PVD NiW coatings. Fig. 1 compares the diffractograms of the different coatings. All the Ni-based coatings deposited either by ED or PVD present a f. c.c. Ni solid solution, as already reported in the literature [29,30]. For the Ni-ED specimen, which was obtained from a sulfamate bath, a marked crystallographic texture along the <100> direction was observed, while for the Ni-PVD, a soft texture along the <111> direction was observed. For both NiW coatings, only one peak associated with the diffraction of the (111) planes was observed. A shift of this peak towards the lower angle was also noticed for the NiW alloys. Tungsten incorporation resulted in a solid solution with a crystalline parameter in the range a = 0.358–0.362 nm, compared to a = 0.352 nm for the Ni coating. The expansion of the lattice parameter with the addition of W is consistent with previous results [31,32]. From Fig. 1, a broadening of the (111) peak was also noticed for the NiW alloys. The grain size ϕ was evaluated using the Scherrer relation. The measured widths were systematically corrected from the instrumental broadening using a NIST reference powder. As shown in Table 1, grain size could be classified as follows: ϕNiW-ED < ϕNiW-PVD < ϕNi-PVD < ϕNi-ED. The Ni-EDcoating was more micrometric compared to the other materials. More-over, due to the larger FWHM (full width at half maximum) value for Ni-PVD, the use of the Scherrer relation was at the limit of validity. For electrodeposition, incorporation of tungsten induced a sharp decrease in grain size, as reported in several studies [29,33,34]. For PVD coatings, the grain size dependence on composition was less pronounced, in accordance with the literature [29,35]. Table 1 also presents the major orientation revealed by the XRD analyses. It seems that when grain size was reduced below 50 nm, the main (111) orientation was similar for all the coatings.

Surface roughness and the morphological aspects of the different coatings were investigated by AFM (Fig. 2). The Ni-ED coating showed a pyramidal-shaped morphology with coarse grains, in agreement with XRD results. The other coatings had a nodular-shaped morphology with very small nodules, consistent with a nanocrystalline microstructure. Electrodeposited pure nickel coatings had a higher roughness that is associated with pyramidal morphology and coarse grains. For the PVD nickel coatings and both ED and PVD NiW coatings, roughness was lower and quite similar (Ra around 10 nm).

These results concerning grain size and shape can be compared to previous ones obtained in Ref. [36] for ED coatings and [21] for PVD coatings. It was shown that using the Scherrer relationship leads to an underestimation of grain size, in particular for low tungsten content alloys. However, TEM offers the opportunity to separate grain size from twin spacing. Thus, the grain size values deduced from this technique were taken as a reference. A grain size of around 200 nm was measured for pure electrodeposited nickel, while the lowest grain size (5 nm) was measured for the Ni–W alloy with 18 at% W. TEM micrographs showed that Ni and low W content alloys displayed numerous twins, which could explain the under estimation of grain size deduced from the Scherrer equation for these coatings. However, for the Ni–W alloy with 15 at% W, an identical grain size was obtained by TEM and XRD and the grain size range was the same as in the present study, i.e. 8 nm for the NiW15 ED and 750 nm for the Ni ED. These values compare well with our results. Concerning the PVD coatings [21], a uniform

nanocrystallline structure for NiW15 with a mean grain size of around 15 nm was obtained, and for the pure nickel coating, nodules of less than 150 nm in height overlaid acompact layer which was formed of smaller nodules. However, the grain size obtained by both TEM and XRD was 16 nm for Ni and 15 nm for NiW15.

Concerning the variation in texture, the results obtained here for the Ni ED coatings are in good agreement with the work of Godon [37]. Indeed, in the latter case, for a similar pure Ni coating obtained by electrodeposition in a sulfamate bath, there was no evidence of twin formation and the strong texture along the 1 0 0 direction was associated with a non-inhibited growth of crystals. The development of a crystal-lographic texture along the 1 1 1 direction was also observed in Ref. [33] for a tungsten content higher than 10 at% and grain sizes below 20 nm. This variation correlated with a decrease in interstitial solute content above 10 at% W. However, for PVD coatings, similar results were ob-tained in Ref. [21]. A uniform nanocrystalline structure and a nodular morphology were obtained. No marked crystallographic texture was observed as the texture index was less than 2 for all the crystallographic directions. It was concluded that the grain size of the coatings was well below the size of the surface nodules deduced from AFM, suggesting that these nodules are composed of a large number of grains.

The contamination of the coatings (Table 1) was investigated using several experimental tools as it is well known that the incorporation of contaminants can modify the microstructure and the properties of coatings. μ-XRF experiments revealed contamination by Iron and Argon in PVD coatings. The slight contamination by iron probably originates from the deposition chamber. The increase in the contamination by argon for the NiW-PVD coating compared with the pure Ni coating is probably due to a higher bombardment of the substrate by high-energy particles from the plasma [22,38,39]. It is well known that electrode-position can lead to the incorporation of light elements due to the chemical species of the plating bath [33,40], and hot extraction analysis was used to evaluate the amount of light elements in ED coatings. The results showed that pure Nickel coating obtained from an additive-free sulfamate bath had very low contamination levels. For NiW-ED, higher contamination levels were obtained, which may be explained by the presence of citrate and tungstate species in the electrodeposited bath [33]. To evaluate the distribution of the species in the coatings, SIMS profiles were performed on the NiW coatings (not shown). Theserevealed a uniform distribution of the elements for both coatings. Moreover, even for the light elements, the intensity of the signals was quite similar for both samples, suggesting similar levels of impurities, except for Argon and Iron. It thus can be concluded that the difference in contamination between the NiW coatings was mainly due to Iron and Argon, the PVD coating containing higher amounts of these impurities, as indicated in Table 1.

Hardness and the Young's Modulus were deduced from instrumented indentation measurements. The results are presented in Fig. 3. Thesearameters are an average value from 12 measurements performed in the same conditions. Starting with the hardness value H, there is a clear classification of the different materials: HNiW-PVD (920 HV) > HNiW-ED (740 HV)> HNi-PVD (560 HV)> HNi-ED (310 HV). This classification is in good agreement with the results in the study of Lagarde [29], in which the experimental conditions induced a significant contribution of the substrate. In our study, a maximum of 10% penetration depth of the coating thickness was chosen to avoid any influence from the substrate. These results can first be analysed based on both grain size and W incorporation effects. Considering first the pure nickel coatings, it was observed that HNi-PVD > HNi-ED. This variation in hardness could be correlated mainly with the effect of grain size, even if other metallur-gical parameters were

different between the pure nickel coatings. Grain size variation conformed to the Hall-Petch relationship that links in-crease in hardness to grain size reduction, especially in this grain size range (from micrometric to relatively large nanometric dimensions >20–50 nm) [29,41,42]. For the NiW alloys, an increase in hardness was observed compared with pure nickel, so HNiW-PVD > HNi-PVD and HNiW-ED >HNi-ED. This was already discussed by ShakibiNia et al. and Lagarde et al. [29,31] and may be principally associated with the solute effect due to tungsten incorporation. Actually, the W element, which sub-stitutes for Ni in the solid solution, may be responsible for such behav-iour [43]. In addition, the microstrain in the coatings may also be involved in the variation in hardness when the W concentration increased [29,43]. However, as grain size was also reduced for both NiW coatings compared to Ni coatings, it may also play a role in the variation in hardness, whatever the elaboration process.

Finally, HNiW-PVD > HNiW-ED. For these two coatings, the main differencearose from grain size, which is smaller for the ED coating, and contamination by Ar and Fe, which is higher in PVD coatings. Thus, the difference in hardness may be related to the breakdown of the Hall-Petch law. Indeed, grain size for NiW-ED was in the range <10–20 nm, which is known to show such a decrease or stabilization of hardness when the grain size diminishes [23,29,44,45]. Thereafter, the high level of argon, notably in the PVD NiW coatings, could also be responsible for the increase in hardness, as discussed in Ref. [39].

Fig. 3 also presents the Young's Modulus values obtained from the instrumented indentation measurements. It is clearly shown that the incorporation of W into the Ni matrix led to a decrease in the Young's Modulus, suggesting a decrease in stiffness. The value dropped from about 240 GPa for the Ni coatings to less than 200 GPa for the NiW alloys. This behaviour was observed both with the PVD and the ED elaboration routes. As already mentioned, the solid solution containing 15 at% W had a lattice parameter of around 0,360 nm compared to 0,352 nm for the pure Ni coating. The decrease in the Young's Modulus value may be attributed to the solid solution effect. Indeed, elastic modulus is known to be linked more specifically to the binding energy between the elements which constitute the material. When W substitutes for Ni in the metallic matrix, the intermetallic combination of a transition element (e.g. W, Mo), which has a partially filled d orbital, and a metal (e.g. Ni, Co), which has fully coupled d electrons, led to asignificant modification of their binding energy [21]. As a consequence, the incorporation of W induced an increase in the interatomic distance. The Young's Modulus, which is proportional to the inverse of the interatomic distance, led to decreased stiffness with W incorporation [46].

3.2. Scratch resistance

Different parameters were measured based on the scratch experi-ments: the depth profiles Pd and Rd respectively during and after loading, and the friction coefficient (Fig. 4). Scratched surfaces were observed both in parallel (Fig. 5) and in a cross-section view (Fig. 6). It can be seen from Fig. 6 outside the scratch tracks that the expected coating thickness of 10 μm was respected.

As a first observation, for the 4 types of coating, the depths Pd increased progressively under loading. The range was 10–20 μm at the end of the experiment, which corresponds mainly to the deformation of the steel substrate. Indeed, the latter was tested in the same mechanical conditions, and the results are in line with such depth values (not shown). Scratch data under final loading are presented in Table 2.

Starting with the Ni-ED coating on steel, both Pd and Rd increased linearly as the load increased, and the two curves overlapped (Fig. 4a). Thus, the depth after loadings Rd was

similar to the depth under loading Pd throughout the scratch test. A strong breakdown in the slope was also observed in friction force variation for a load of less than 10 N, which is a sign of coating breakdown and/or abrasion [47,48]. Moreover, from Figs. 5a and 6a, the abrasion of the coating is also clear. Two opposite phenomena may explain this result. On the one hand, the steel substrate was deformed, which led to its elastic recovery, and on the other hand, the coating was abraded, decreasing its thickness. Thus, the elastic re-covery of the substrate was compensated by the coating abrasion or erosion which led to roughly the same values for Pd and Rd. In addition, some pile-ups were visible in front and on the sides of the scratch (Fig. 5a), which is a sign of displacement of material. An almost com-plete abrasion of the coating was observed at the end of the experiment for the highest load (Fig. 6a). Finally, deformation of the substrate and abrasion of the coating were found for a soft Ni-ED coating on a rela-tively soft steel substrate. For the Ni-PVD coating on steel (Fig. 4b), Rd and Pd increased linearly with load; Rd depths were slightly lower than Pd depths during the whole scratch experiment, indicating an elastic recovery. An inflection was also observed in the variation in friction force for a load of about 15 N, which is compatible with a partial con-sumption of the coating. In this case, an elastic recovery of the substrate occurred, but it was at least partially compensated by the abrasion or break-down of the coating throughout the scratch test (Figs. 5b and 6b). This is the case of a hard coating on a soft substrate [49]. The coating seemed to accommodate the substrate deformation only for the lowest load, then pile-ups also appeared, which indicates plastic deformation of the coating and abrasion (Fig. 6b), leading to a gradual reduction in thickness.

Although the Ni-ED coating had a submicrometric grain size compared to the Ni-PVD, whose grain size is about 50 nm, both coatings generally showed similar trends and some evidence of abrasive wear. However, the Ni-ED coating had no defects inside the scratch, but a lot of accumulation of material at the lateral and final edge of the scratch (Fig. 5a). This confirms a displacement of material in front of the tip and thus the ductile character of the coating. Ni-PVD behaved quite simi-larly. However, the lateral edges were more marked with, for example, chipping and some cracks at the end of the scratch for the highest load (Fig. 5b).

Concerning the NiW-ED coatings on steel, the depth under loading Pdincreased almost linearly up to about 20 N. Given the variations for Rd and Pd during the whole scratch test (Fig. 4c), a strong elastic recovery was found. The variation in friction force showed no signs of variation in slope, which seems compatible with the absence of breakdown or abrasion of the coating. NiW-ED coating perfectly followed the substrate deformation for all applied loads (Fig. 6c). The adhesion between coating and substrate was unaltered (Figs. 5c and 6c). In addition, the residual thickness of the coating in the middle of the scratch at the end of the test was quite similar to the original. Thus, an elastic recovery of both the substrate and the coating was clear throughout the experiment. No sign of breakdown or abrasion was observed, meaning that the coating could accommodate the substrate deformation throughout the test. The hardness of the coating was significant in this case (740 HV), higher than for the Ni- ED or PVD coatings. As previously mentioned for the variation in hardness, the grain size (<10 nm) for the NiW-ED coating was compatible with a breakdown of the Hall-Petch law, and the incorporation of W may promote grain boundary sliding mecha-nisms in the deformation process [23,50]. Thus, it seems that the ability of the material to deform without breaking was enhanced. Also, and as a consequence, the adhesion between the coating and the substrate was preserved.

The NiW-PVD coating on a steel substrate was also investigated (Figs. 4d, 5d and 6d). Clearly, as for NiW-ED, a high elastic recovery of both the substrate and the coating was

observed. In addition, the friction coefficient was continuous, with no marked variation in the slope. This means that there was not even a partial breakdown of the coating. In this case, the coating followed the substrate deformation until the end of the scratch test. So, as for the NiW-ED material, the coating was still present at the end. As previously shown, it was the hardest coating, but the grain size was not the lowest, at around 20 nm. The PVD coating hardness was also related to the main role played by the Ar impurity [39], which brought a brittle character to the alloy. Optically, NiW-PVD coatingchippings (Figs. 5d and 6d). However, compared to Ni-PVD, there was less accumulation of material, indicating a beneficial effect of tungsten incorporation. The adhesion between the substrate and the coating was also well preserved at the end of the scratch test.

3.3. Tribological behaviour

The different coatings were tested in pin-on-disk experiments in air. The friction force and wear volume (from profilometry measurements) were evaluated (Figs. 7 and 8). In addition, the worn surfaces were observed and analysed by optical microscopy and micro-Raman spec-troscopy (Figs. 9 and 10).

Starting with the friction coefficient measurements, Fig. 7 presents the results obtained for the different coatings. The experiments were conducted twice and the reproducibility was good. Both Ni-ED and PVD increased rapidly (1–10 laps) towards high friction values (μ = 0,75-1), while for both NiW-ED and PVD, two regimes of friction could be distinguished. A low friction regime (μ ranging from 0,25 to 0.35) with a duration of between 100 and 1000 laps before a high friction domain was attained (μ > 0.75). This kind of low to high regime of friction behaviour was already found with nanocrystalline metallic materials [51,52]. It was indeed shown that when the grain size range is not far from a critical value (usually around 10–20 nm), it may induce an initial low period of friction which involves mainly grain boundary plasticity. During this low period of friction, the grain microstructure usually be-comes coarser, and finally attains a high friction regime, which is more compatible with intragranular plasticity [53]. In the present study, the grain size of both NiW-PVD and NiW-ED was in the range 8–20 nm, which is in good agreement with the above description.

On the other hand, for Ni-ED and Ni-PVD coatings with a grain size > 50 nm or even a submicrometric size, for Ni-ED (750 nm), only a high friction regime was observed. Finally, concerning friction behaviour, there was no clear distinction between PVD and the ED processes for Ni and NiW. ts after 10 000 laps (Fig. 8). In order to discuss the variation in wear volume as a function of the study parameters, the wear rate k is more frequently used in the literature. This can be calculated using the following equation (more details are given in Table 3):

$$k = \frac{V}{Fs}$$

V represents the wear volume (mm3), F the normal load (N) and s the total sliding distance (m).

Moreover, the wear track depth and width were measured by pro-filometry. The track depth and width were comparable for the Ni-ED and Ni-PVD coatings: in the 6–8 μm range for depth and 400–500 μm for width. However, the wear profiles had different shapes, with a sharp inflexion for Ni-ED, which is a sign of progressive abrasion, while for Ni- PVD the center of the track was raised, which may correspond to debris accumulation or the formation of a tribofilm in the track [53–55]. On the other hand, the wear profiles were very different for the

NiW-ED and NiW-PVD coatings. Indeed, the track widths were <200 µm, and the track depth was inferior to 1 µm, mainly at the limit of the profilometer resolution. In this case also, the two deposition processes, ED and PVD, led to similar behaviour. As these two materials are harder (740 HV for NiW-ED and 920 HV for NiW-PVD, respectively) than Ni-ED (300 HV) and Ni-PVD (550 HV), such behaviour is also compatible with a wear volume which varies with the inverse of hardness [56]. Although hardness is an important parameter in wear resistance, some authors proved that the ratio of hardness and elastic modulus is a suitable parameter to better define wear resistance [57,58]. Leyland and Mat-thews [59] suggested that a coating with the highest hardness and highest H/E ratio provides the highest resistance to plastic deformation. In our case, the NiW coatings had a higher wear resistance (with 15 at.% W), as seen in Table 3.

Fig. 9 presents the images of the wear tracks for the 4 coatings. As shown by the profilometry measurements, the wear tracks were signif-icantly larger for the Ni-ED and Ni-PVD coatings than for NiW. In addition, numerous worn products and debris were visible both in the wear tracks and beside the Ni coatings, while for the NiW materials, yellow and orange products were visible next to the wear tracks.

Finally, Fig. 10 groups the Raman spectra obtained for the four materials from the analyses of both the wear tracks and the counterbody worn pin. For the Ni-ED and Ni-PVD materials, nickel oxides and a very small quantity of iron oxides were found on the worn surfaces, both in the wear tracks and on the pin. The latter corresponds mainly to a transfer film formed on the pin. On the other hand, nickel and tungsten. oxides were observed on the wear tracks of the NiW-ED and NiW- PVD coatings. However, on the pin, in addition to these two oxidation products from the coatings, some additional vibration bands were visible around 1300 to 1600 cm 1 and may be assigned to iron oxides and mixed oxides [55,60].

The 100 Cr6 steel pin is a hard material (around 800 HV). Thus, for both the ED-Ni and PVD-Ni coatings, a tribo-contact was involved be-tween a hard material (the pin) and a relatively soft one (the Ni coat-ings). This seems to lead mainly to abrasive wear, with numerous and deep contact asperities formed in the soft Ni coatings. Thus, the result was significant abrasive wear with the formation of mainly tribo- oxidation products from the Ni coatings. This induced the formation of a transferred film on the pin. On the other hand, for the NiW-ED and NiW-PVD coatings, there is contact between two hard materials. The wear mechanism seemed to be mainly adhesive, with asperity contacts formed between the coating and the pin, thus giving rise to worn par-ticles from the two antagonist materials. Consequently, tribo-oxidation products originating from both the steel pin and the NiW coatings were formed. However, since the antagonists have roughly the same hardness values, the number and depth of the contact asperities were largely reduced, which resulted in a very low wear rate.

4 conclusion

In the present work, many analyses were carried out on the surface mechanical characteristics of Ni and NiW coatings produced by elec-troplating (ED) and sputtering (PVD). Hardness and Young's Modulus values were extracted, and abrasion and wear resistance were detailed. Furthermore, the main microstructural features were investigated simultaneously to highlight the role played by W incorporation, and showed the influence of the ED and PVD processing routes for andentical W content of 15 at. %. The main results obtained were:

All the Ni-based coatings deposited either by ED or PVD had a f. c.c. Ni solid solution. W incorporation produced a solid solution with a crystalline lattice parameter in the range a

= 0,358–0362 nm compared to a = 0,352 nm for the Ni coatings. The grain size in the Ni-ED coating was more micrometric compared to other materials. For electrodeposi-tion, the incorporation of W induced a significant decrease in grain size, while for the PVD coatings, the dependence of grain size on composition was less pronounced. In addition, when the grain size was reduced to below 50 nm, the main crystallographic orientation (111) was similar for all the coatings. Ni-ED coatings showed a pyramidal-shaped morphology with coarse grains. All the other coatings presented a nodular-shaped morphology with very small nodules, consistent with a nanocrystalline microstructure.

The PVD coatings were contaminated mainly by Argon and Iron, while the Ni-ED coatings obtained here from a sulfamate bath showed very low contamination levels. For the NiW-ED coatings, higher contamination levels by light elements were obtained depending on the presence of citrate and tungstate species in the bath.

The hardness values for the different coatings were significantly different. A clear classification between the different materials was demonstrated: HNiW-PVD (920 HV) > HNiW-ED (740 HV) > HNi-PVD (560 HV) > HNi-ED (310 HV). The results were analysed for both grain size and W incorporation effects. However, in addition, the high level of Argon, in particular for the NiW-PVD coating, was found to be responsible for the highest hardness value obtained. W incorporation in the Ni matrix also led to a decrease in the Young's Modulus.

Abrasion resistance and adhesion were investigated through scratch measurements and tribological tests. During scratch formation, both NiW coatings closely followed substrate deformation without a sign of abrasion, and a total absence of breakdown was observed only for the NiW-ED coating. Concerning tribological behaviour, an abrasive wear mechanism was clearly shown for both the Ni-ED and Ni-PVD coatings with a corresponding high wear volume. On the other hand, for the NiW- ED and NiW-PVD coatings, the wear mechanism seemed to be mainly adhesive.

CRediT authorship contribution statement

D. Figuet: Conceptualization, Data curation, Formal analysis, Investigation, Methodology, Software, Visualization, Writing, Writing – original draft. A. Billard: Data curation, Resources. C. Savall: Formal analysis, Funding acquisition, Investigation, Methodology, Project administration, Resources, Supervision, Validation. J. Creus: Formal analysis, Funding acquisition, Investigation, Methodology, Project administration, Resources, Supervision, Validation, Visualization. S. Cohendoz: Data curation, Formal analysis, Investigation, Methodology. J.L. Grosseau-Poussard: Conceptualization, Formal analysis, Investi-gation, Methodology, Project administration, Supervision, Validation, Visualization, Writing, Writing – original draft.

Declaration of competing interest

The authors declare that they have no known competing financial interests or personal relationships that could have appeared to influence the work reported in this paper.

Acknowledgments

The authors would like to thank the Nouvelle Aquitaine Region for their financial support, and Dr. E. Conforto and C. R´eb´er´e (from LaSIE, CNRS UMR 7356,ULR, F-17000 La Rochelle, France) for their help in obtaining SEM and μ-X-ray fluorescence spectroscopy data, respectively.

References

[1] N. Alharthi, E.-L.M. Sherif, H.S. Abdo, S.Z. El Abedin, Effect of nickel content on the corrosion resistance of iron-nickel alloys in concentrated hydrochloric acid pickling solutions, Hindawi - Adv. Mater. Sci. Eng. 2017 (2017) 8.

[2] A. Bahramian, M. Eyraud, F. Vacandio, P. Knauth, Improving the corrosion properties of amorphous Ni-P thin films using different additives, Surf. Coating. Technol. 345 (2018) 40–52.

[3] J. Yu, Y. Wang, X. Zhao, Q. Li, Q. Qiao, J. Zhao, S. Zhai, Wear resistance of Ni-based alloy coatings, Hindawi - Adv. Mater. Sci. Eng. 2019 (2019) 7.

[4] H.B. Lee, Synergy between corrosion and wear of electrodeposited Ni-W coating, Tribol. Lett. 50 (2013) 407–419.

[5] A.R. Jones, I.J. Hamann, A.C. Lund, C.A. Schuh, Nanocrystalline Ni-W Alloy Coating for Engineering Applications, Plating & Surface Finishing, 2010,

pp. 53–60.

[6] N.P. Wasekar et, G. Sundararajan, Sliding wear behavior of electrodeposited Ni-W alloy and hard chrome coatings, Wear 342–343 (2015) 340–348.

[7] A.K. Basak, J.-P. Celis, P. Ponthiaux, F. Wenger, P. Matteazzi, M. Vardavoulias, Effect of nanostructuring and alloying element on electrochemical behaviour of HVOF sprayed WC-Co coatings, J. Electrochem. Soc. 56 (2009).

[8] M. Ciurdaș, R.E. Dumitrescu, G. Popescu, D.A. Necsulescu, A.M. Predescu, C.

M. Pantilimon, L. Rosu, Nanocrystalline and amorphous NiTi compound obtained by mechanical alloying for metallic matrix reinforcement, Int. J. Mod. Manuf. Technol. n◦ 2 (2018).

[9] T. Raghu, R. Sundaresan, P. Ramakrishnan, T.R. Rama Mohan, Synthesis of nanocrystalline copper–tungsten alloys by mechanical alloying, Mater. Sci. Eng., A 304–306 (2001) 438–441.

[10] K.-H. Hou, Y.-F. Chang, S.-M. Chang, C.-H. Chang, The heat treatment effect on the structure and mechanical properties of electrodeposited nano grain size Ni–W alloy coatings, Thin Solid Films 518 (n◦24) (2010) 7535–7540.

[11] M.V.N. Vamsi, N.P. Wasekar, G. Sundararajan, Influence of heat treatment on microstructure and mechanical properties of pulse electrodeposited Ni-W alloy coatings, Surf. Coating. Technol. 319 (2017) 403–414.

[12] A.J. Detor, M.K. Miller, C.A. Schuh, Solute distribution in nanocrystalline NiW alloys examined through atom probe tomography, Phil. Mag. 86 (28) (2006) 44594475.

[13] M.P. Quiroga Arga˜naraz, S.B. Ribotta, M.E. Folquer, E. Zelaya, C. Llorente,

J. Ramallo-Lopez, G. Benítez, A. Rubert, L.M. Gassa, M.E. Vela, R.C. Salvarezza, The chemistry and structure of nickel-tungsten coatings obtained by pulse galvanostatic electrodeposition, Electrochim. Acta 72 (2012) 8793.

[14] K.R. Sriraman, S. Ganesh Sundara Raman, S.K. Seshadri, Corrosion behaviour of electrodeposited nanocrystalline Ni–W and Ni–Fe–W alloys, Mater. Sci. Eng., A 460– 461 (2007) 39–45.

[15] N.P. Wasekar, N. Hebalkar, A. Jyothirmayi, B. Lavakumar, M. Ramakrishna, Influence of pulse parameters on the mechanical properties and electrochemical corrosion behavior of electrodeposited Ni-W alloy coatings with high tungsten content, Corrosion Sci. 165 (2020).

[16] C. Borgia, T. Scharowsky, A. Furrer, C. Solenthaler, R. Spolenak, A combinatorial study on the influence of elemental composition and heat treatment on the phase

composition, microstructure and mechanical properties of Ni–W alloy thin films, Acta Mater. 59 (n◦ 1) (2011) 386–399.

[17] L. Zhu, O. Younes, N. Ashkenasy, Y. Shacham-Diamand, E. Gileadi, STM/AFM studies of the evolution of morphology of electroplated Ni/W alloys, Appl. Surf. Sci. 200 (n 1–4) (2002) 1–14.

[18] A. Billard, F. Maury, P. Aubry, F. Balbaud-C´el´erier, B. Bernard, F. Lomello, H. Maskrot, E. Meillot, A. Michau, F. Schuster, Emerging processes for metallurgical coatings and thin films, Compt. Rendus Phys. 19 (n◦8) (2018) 755–768.

[19] A. Kawashima, E. Akiyama, H. Habazaki, K. Hashimoto, Characterization of sputter- deposited Ni-Mo and Ni-W alloy electrocatalysts for hydrogen evolution in alkaline solution, Mater. Sci. Eng., A 226–228 (1997) 905–909.

[20] M. Metikoˇs-Hukovi´c, Z. Grubac, N. Radic, A. Tonejc, Sputter deposited nanocrystalline Ni and Ni-W films as catalysts for hydrogen evolution, J. Mol. Catal. Chem. 249 (n◦1- 2) (2006) 172–180.

[21] M. Lagarde, A. Billard, J. Creus, X. Feaugas, J.-L. Grosseau-Poussard, S. Touzain, C. Savall, Electrochemical behaviour of Ni-W alloys obtained by magnetron sputtering, Surf. Coating. Technol. 352 (2018) 581–590.

[22] M.H. Allahyarzadeh, M. Aliofkhazraei, A.R. Rezvanian, V. Torabinejad, A. R. Sabour, Rouhaghdam« Ni-W electrodeposited coatings: characterization, properties and applications, Surf. Coating. Technol. 307 (2016) 978–1010.

[23] A.C. Mishra, A.K. Thakur, V. Srinivas, Effect of deposition parameters on microstructure of electrodeposited nickel thin films, J. Mater. Sci. 44 (n◦13) (2009) 3520–3527.

[24] J.A. Thornton, High rate thick film growth, Annu. Rev. Mater. Sci. 7 (1977) 239–260.

[25] A. Billard, F. Perry, « Pulv´erisation Cathodique », Techniques de l'Ing´enieur, 2005.

[26] T. Yamasaki, P. Schloβmacher, K. Ehrlich, Y. Ogino, Formation of amorphous electrodeposited Ni-W alloys and their nanocrystallization, Nanostruct. Mater. 10 (n◦3) (1998) 375–388.

[27] W.C. Oliver, G.M. Pharr, An improved technique for determining hardness and elastic modulus using load and displacement sensing indentation experiments, J. Mater. Res. 7 (n◦ 6) (1992).

[28] N. Bader, F. Pape, H.H. Gatzen, G. Poll, Examination of friction and wear of a 100Cr6 ball against a bearing ring in a micro-pin-on-disk tester, WIT Trans. Eng. Sci. 91 (2015).

[29] M. Lagarde, Relations proc´ed´es d''elaboration, ´etat m´etallurgique, propri´et´es des alliages nanostructur´es de Ni-W, PhD Thesis, La Rochelle Universit´e, La Rochelle, France, 2017.

[30] E. Vernickaite, N. Tsyntsaru, K. Sobczak, H. Cesiulis, Electrodeposited tungsten-rich Ni-W, Co-W and Fe-W cathodes for efficient hydrogen evolution in alkaline medium, Electrochim. Acta 318 (2019) 597–606.

[31] N. Shakibi Nia, C. Savall, J. Creus, J. Bourgon, P. Girault, A. Metsue, S. Cohendoz, X. Feaugas, On the implication of solute contents and grain boundaries on the Hall- Petch relationship of nanocrystalline Ni-W alloys, Mater. Sci. Eng., A 678 (2016) 204–214.

[32] L.T. Kong, J.B. Liu, W.S. Lal, B.X. Liu, Correlation of lattice constant versus tungsten concentration of the Ni-based solid solution examined by molecular dynamics simulation, J. Alloys Compd. 337 (2002) 143–147.

[33] N. Shakibi Nia, J. Creus, X. Feaugas, C. Savall, The effect of tungsten addition on metallurgical state and solute content in nanocrystalline electrodeposited nickel,
J. Alloys Compd. 609 (2014) 296–301.
[34] A. Chianpairot, G. Lothongkum, C.A. Schuh, Y. Boonyongmaneerat, « Corrosion of nanocrystalline Ni-W alloys in alkaline and acidic 3.5 wt.% NaCl solutions, Corrosion Sci. 53 (2011) 1066–1071.
[35] T.J. Rupert, J.C. Trenkle, C.A. Schuh, Enhanced solid solution effects on the strength of nanocrystalline alloys, Acta Mater. 59 (2011) 1619–1631.
[36] N. Shakibi Nia, J. Creus, X. Feaugas, C. Savall, Influence of metallurgical parameters on the electrochemical behaviour of electrodeposited Ni and Ni-W nanocristalline alloys, Appl. Surf. Sci. 370 (2016) 149–159.
[37] A. Gaudon, J. Creus, X. Feaugas, E. Conforto, L. Pichon, C. Armand, C. Savall, Characterization of electrodeposited nickel coatings from sulfamate electrolyte without additive, Mater. Char. 62 (2011) 164–173.
[38] C. Paturaud, G. Farges, M.C. Sainte Catherine, J. Machet, Influence of particle energies on the properties of magnetron sputtered tungsten films, Surf. Coating. Technol. 98 (1998) 1257–1261.
[39] C. Paturaud, G. Farges, M.C. Sainte Catherine, J. Machet, Correlation between hardness and embedded argon content of magnetron sputtered chromium films, Thin Solid Films 347 (1999) 46–55.
[40] Y.D. Gamburg, G. Zangari, « Theory and Practice of Metal Electrodeposition », Springer, 2011, p. 385.
[41] H. Kotan, M. Saber, C.C. Koch, R.O. Scattergood, Effect of annealing on microstructure, grain growth, and hardness of nanocrystalline Fe–Ni alloys prepared by mechanical alloying, Mater. Sci. Eng., A 552 (2012) 310–315.
[42] E.N. Hahn, M.A. Meyers, Grain-size dependent mechanical behavior of nanocrystalline metals, Mater. Sci. Eng., A 646 (2015) 101–134.
[43] A. Detor, C. Schuh, Tailoring and patterning the grain size of nanocrystalline alloys, Acta Mater. 55 (n o 1) (2007) 371–379.
[44] T.D. Shen, R.B. Schwarz, S. Feng, J.G. Swadener, J.Y. Huang, M. Tang, J. Zhang, S. C. Vogel, Y. Zhao, Effect of solute segregation on the strength of nanocrystalline alloys: inverse Hall– Petch relation, Acta Mater. 55 (n o 15) (2007) 5007–5013.
[45] K.R. Sriraman, S. Ganesh Sundara Raman, S.K. Seshadri, Synthesis and evaluation of hardness and sliding wear resistance of electrodeposited nanocrystalline Ni–W alloys, Mater. Sci. Eng., A 418 (n o 1- 2) (2006) 303–311.
[46] L. You, X. Song, A study of low Young's modulus Ti–Nb–Zr alloys using d electrons alloy theory, Scripta Mater. 67 (n◦1) (2012) 57–60.
[47] K. Marjolaine, Adhesion Characterization of Hard Ceramic Coatings by the Scratch Test, PhD thesis, Queen's University, Kingston Ontario, Canada, 1999.
[48] K. Khlifi, A. Ben Cheikh Larbi, Investigation of adhesion of PVD coatings using various approaches, Surf. Eng. 29 (n◦7) (2013) 555–560.
[49] J.H. Je, E. Gyarmati, A. Naoumidis, Scratch adhesion test of reactively sputtered TiN coatings on a soft substrate, Thin Solid Films 136 (1986) 57–67.
[50] T.J. Rupert, W. Cai, C.A. Schuh, Abrasive wear response of nanocrystalline Ni–W alloys across the Hall–Petchbreakdown, Wear 298– 299 (2013) 120–126.

[51] N. Argibay, T. Furnish, B.L. Boyce, B.G. Clark, M. Chandross, Stress-dependent grain size evolution of nanocrystalline Ni-W and its impact on friction behavior, Scripta Mater. 123 (2016) 26–29.

[52] N. Argibay, M. Chandross, S. Cheng, J.R. Michael, Linking microstructural evolution and macro-scale friction behavior in metals, J. Mater. Sci. 52 (n◦ 5)
(2017) 2780–2799.

[53] J.F. Panzarino, T.J. Rupert, Concurrent transitions in wear rate and surface microstructure in nanocrystalline Ni-W, Materialia 4 (2018) 38–46.

[54] M. Shafiei, A.T. Alpas, Friction and wear mechanisms of nanocrystalline nickel in ambient and inert atmospheres, Metall. Mater. Trans. 38A (2007) 1621–1631.

[55] A.S.M.A. Haseeb, U. Albers, K. Bade, Friction and wear characteristics of electrodeposited nanocrystalline nickel–tungsten alloy films, Wear 264 (n◦1- 2) (2008) 106–112.

[56] T.J. Rupert, C.A. Schuh, Sliding wear of nanocrystalline Ni-W: structural evolution and the apparent breakdown of Archard scaling, Acta Mater. 58 (2010)
4137–4148.

[57] S. Hong, Y.P. Wu, B. Wang, J.F. Zhang, Y. Zheng, L. Qiao, Nanomechanical properties and dry sliding wear behavior of conventional and nanostructures WC- CoCr coatings prepared by HVOF spraying, Digest J. Nanomater. Biostr. 11 (n◦4) (2016) 1135–1143.

[58] W. Ni, Y.-T. Cheng, M.J. Lukitsch, A.M. Weiner, L.C. Lev, Effects of the ratio of hardness to Young's modulus on the friction and wear behavior of bilayer coatings, Appl. Phys. Lett. 85 (2004) n◦18.

[59] A. Leyland, A. Matthews, On the significance of the H/E ratio in wear control: a nanocomposite coating approach to optimized tribological behaviour, Wear 246 (2000) 1–11.

[60] S.-H. Lee, H.M. Cheong, N.-G. Park, C.E. Tracy, A. Mascarenhas, D.K. Benson, S.
K. Deb, Raman spectroscopic studies of Ni–W oxide thin films, Solid State Ionics 140 (2001) 135–139.

List of figure captions

Fig. 1. XRD diffractograms for the different coatings obtained by both processes: a) Ni-ED; b) Ni-PVD; c) NiW-ED; d) NiW-PVD.

Fig. 2. AFM images of as-deposited coatings: a) Ni-ED; b) Ni-PVD; c) NiW-ED; d) NiW-PVD.

Fig. 3. Evolution of hardness (blue) and Young modulus (orange) for the different coatings obtained by both processes. (For interpretation of the references to colour in this figure legend, the reader is referred to the Web version of this article.)

Fig. 4. Scratch results for Ni and NiW deposits. Data plotted are the friction coefficient μ (red), the depth under loading Pd (blue) and the depth after loading Rd (green), versus the normal load and the displacement along the scratch; a) Ni-ED; b) Ni-PVD; c) NiW-ED; d) NiW-PVD. (For interpretation of the references to colour in this figure legend, the reader is referred to the Web version of this article.)

Fig. 5. SEM top views of the scratchs after progressive loading. This represents the final pile-up along x axis closed to 30 N for the differents coatings: a) Ni-ED; b) Ni-PVD; c) NiW-ED; d) NiW-PVD.

Fig. 6. SEM cross section views of the scratchs after progressive loading. The SEM images correspond to the two chosen loads around 13 and 28 N, for the different coatings: a) Ni-ED; b) Ni-PVD; c) NiW-ED; d) NiW-PVD.

Fig. 7. Evolution of the friction coefficient versus the number of laps: a) Ni-ED; b) Ni-PVD; c) NiW-ED; d) NiW-PVD. Both curves (red and blue) correspond to similar tribology tests with two different wear track radius. (For interpretation of the references to colour in this figure legend, the reader is referred to the Web version of this article.)

Fig. 8. Wear track profiles after the tribological tests: a) Ni-ED; b) Ni-PVD; c) NiW-ED; d) NiW-PVD.

Fig. 9. Optical top views of the worn coatings after sliding in air against a 100 Cr6 ball under 1 N: a) Ni-ED; b) Ni-PVD; c) NiW-ED; d) NiW-PVD.

Fig. 10. Micro-Raman spectra of the worn products on coatings (blue) and on pin (orange) after 10 000 laps: a) Ni-ED; b) Ni-PVD; c) NiW-ED; d) NiW-PVD. (For interpretation of the references to colour in this figure legend, the reader is referred to the Web version of this article.)

List of Tables caption

Table 1 Summary of microstructural features and chemical properties of Ni and Ni–W alloys. Deposits classified as a function of tungsten content, crystallographic texture, grain size, roughness and impurities content.

Table 2 Scratch data of different coatings at final loading (F = 29–30 N).

Table 3 Wear rates and H/E ratios of different coatings.

List of figures

Fig 1

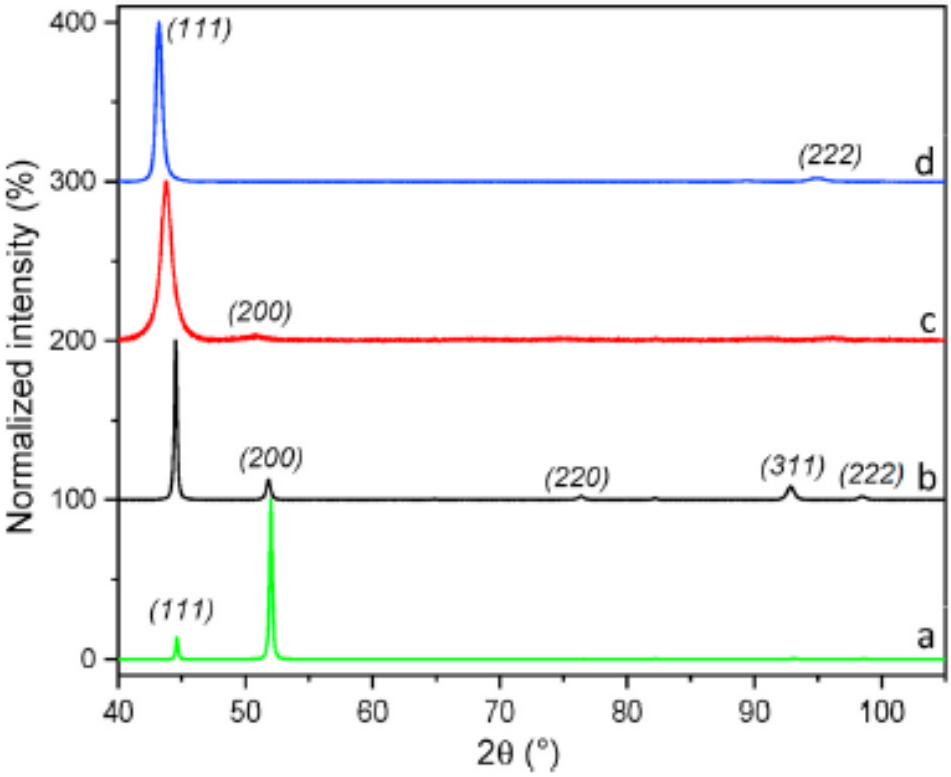

Fig2

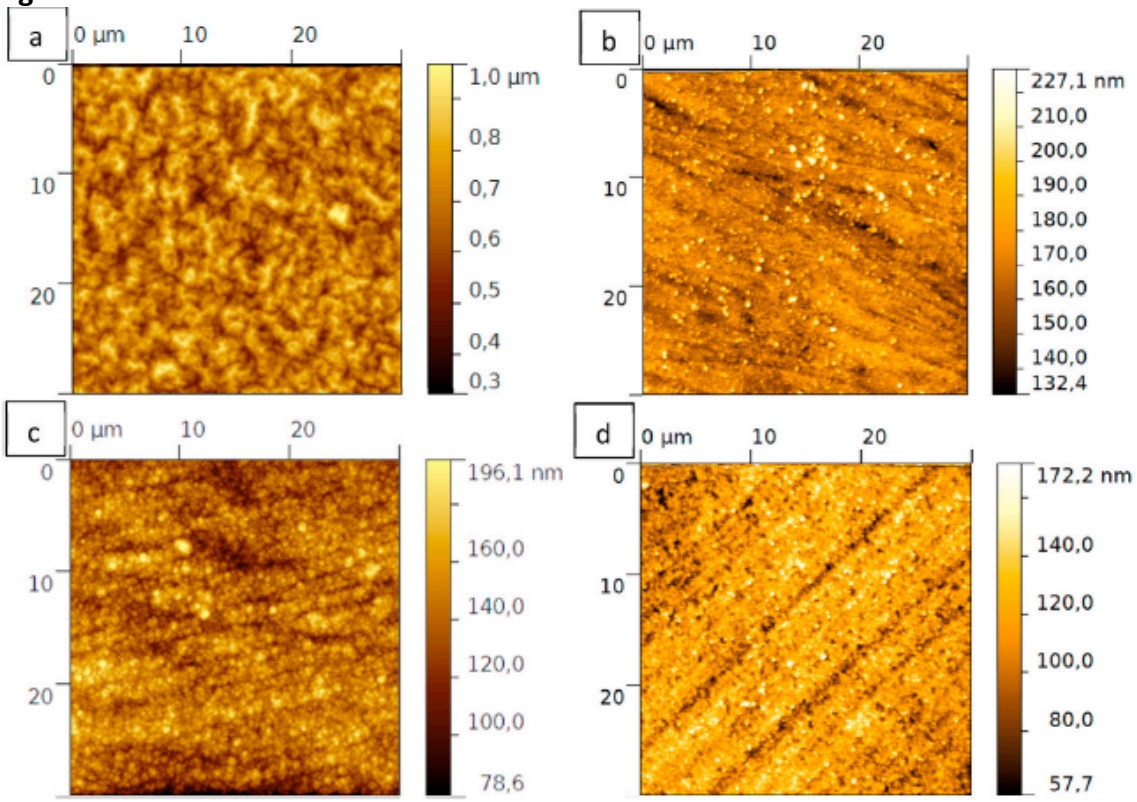

Fig 3

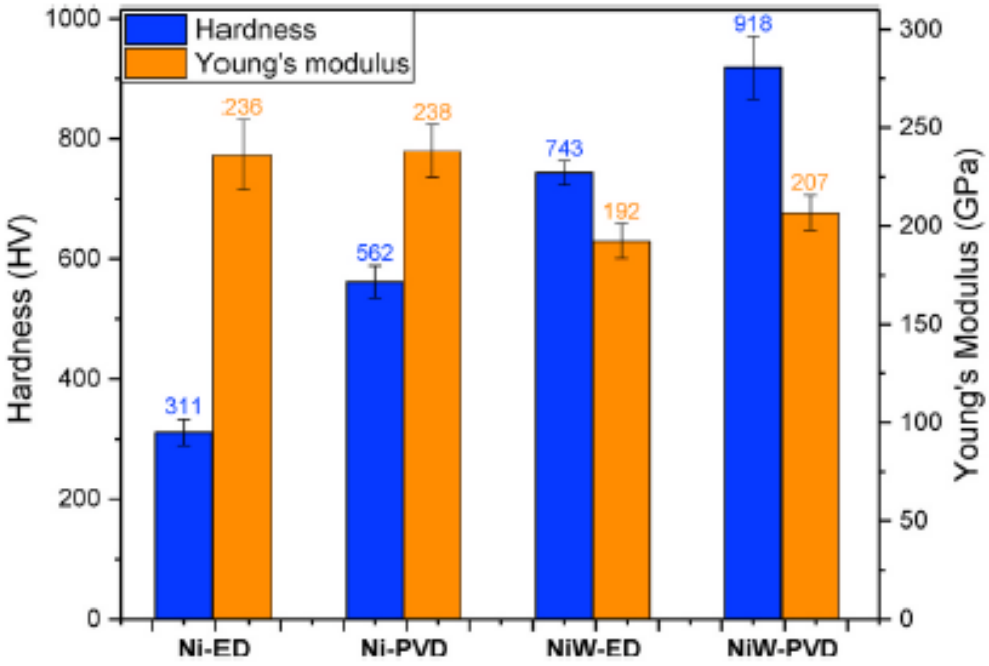
Hardness
Young's modulus
Hardness (HV)
Young's Modulus (GPa)
311
236
562
238
743
192
918
207
Ni-ED
Ni-PVD
NiW-ED
NiW-PVD

Fig 4

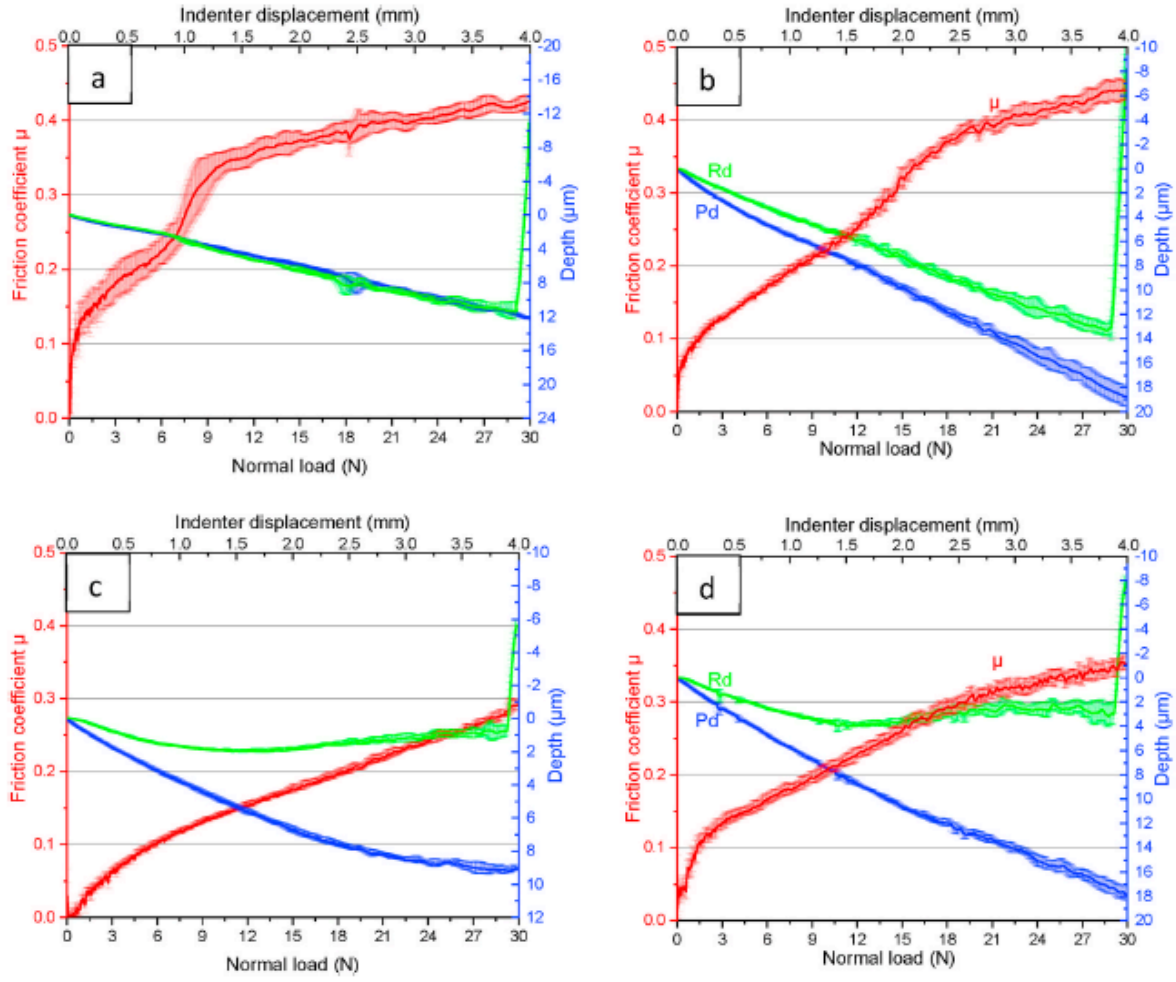
a
b
c
d
Indenter displacement (mm)
Friction coefficient μ
Depth (μm)
Normal load (N)
μ
Rd
Pd

Fig 5

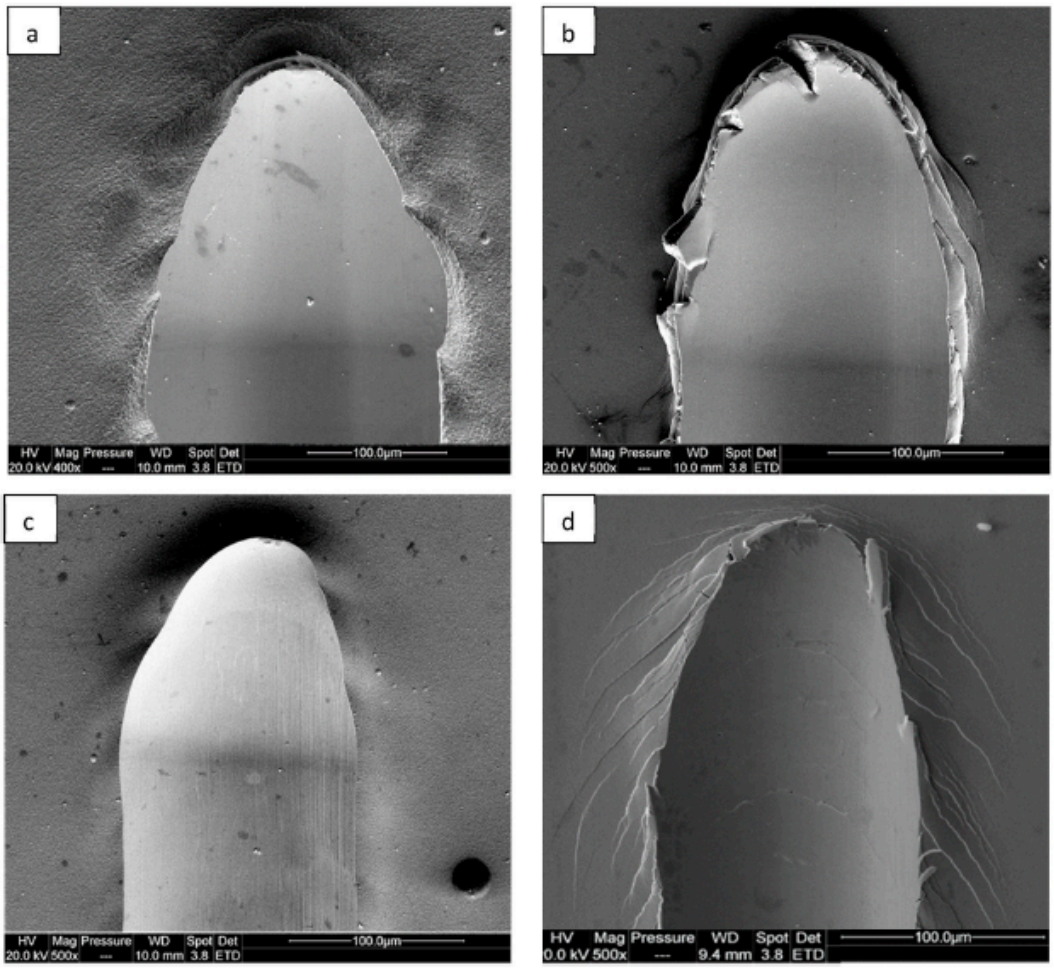

Fig 6

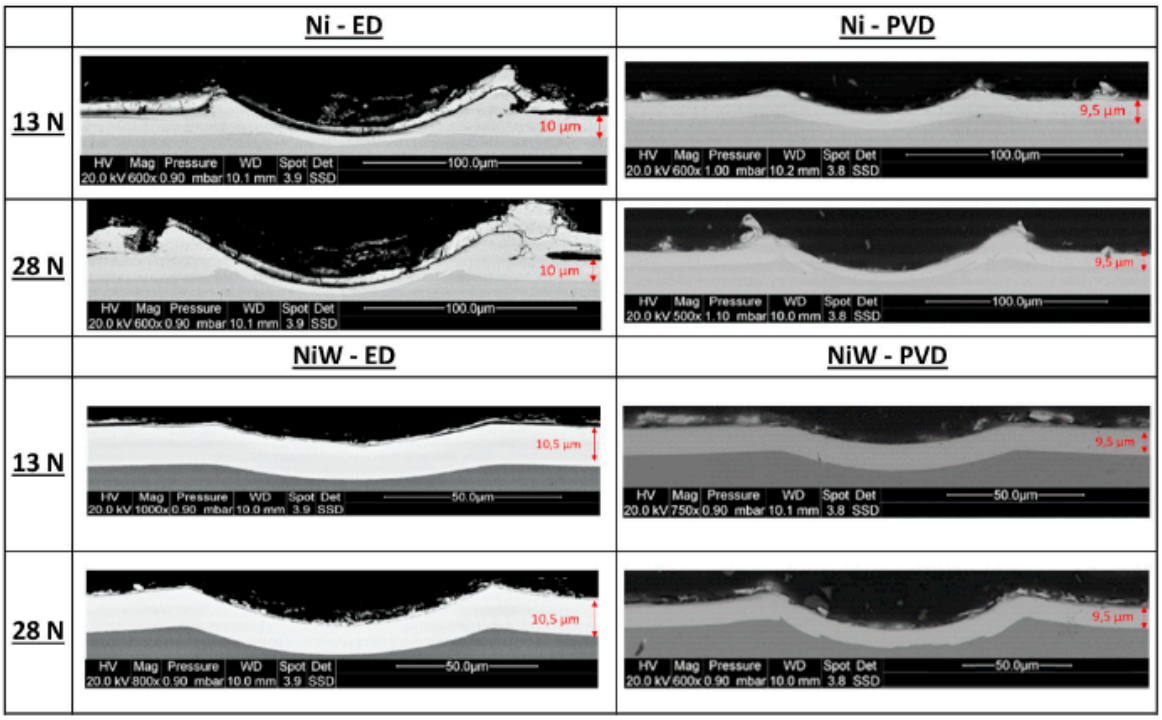

Fig 7

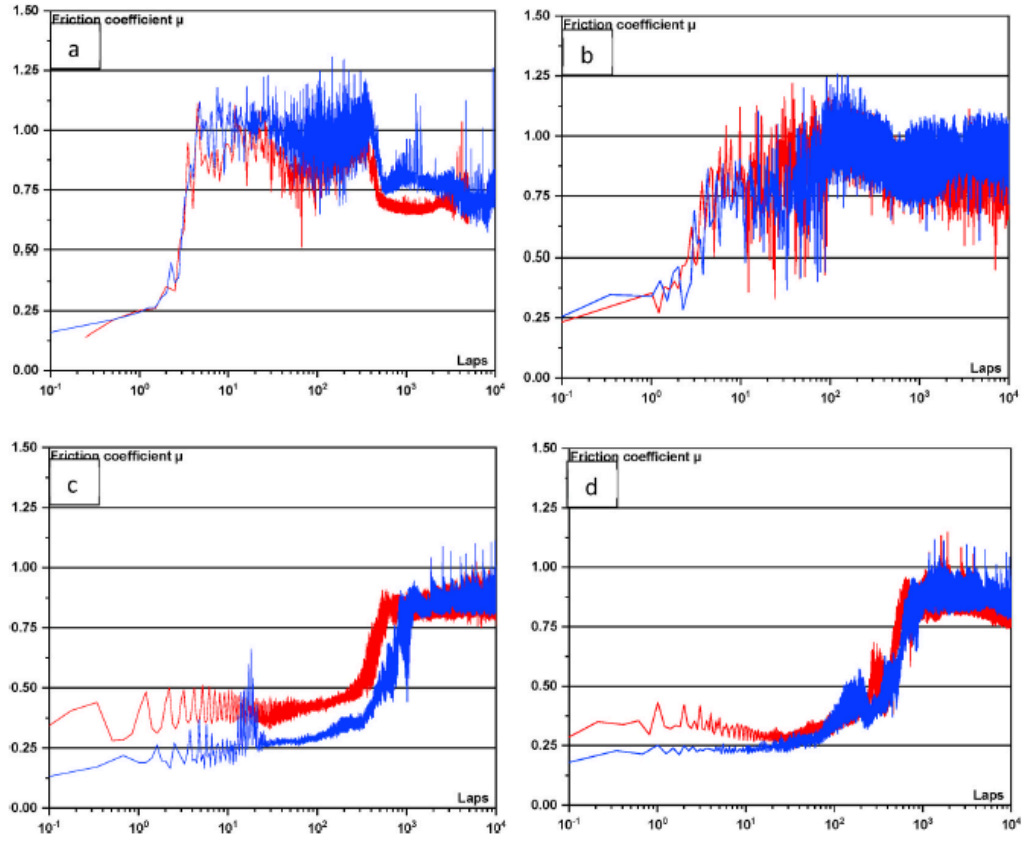
Friction coefficient μ
a
b
c
d
Laps
1.50
1.25
1.00
0.75
0.50
0.25
0.00

Fig 8

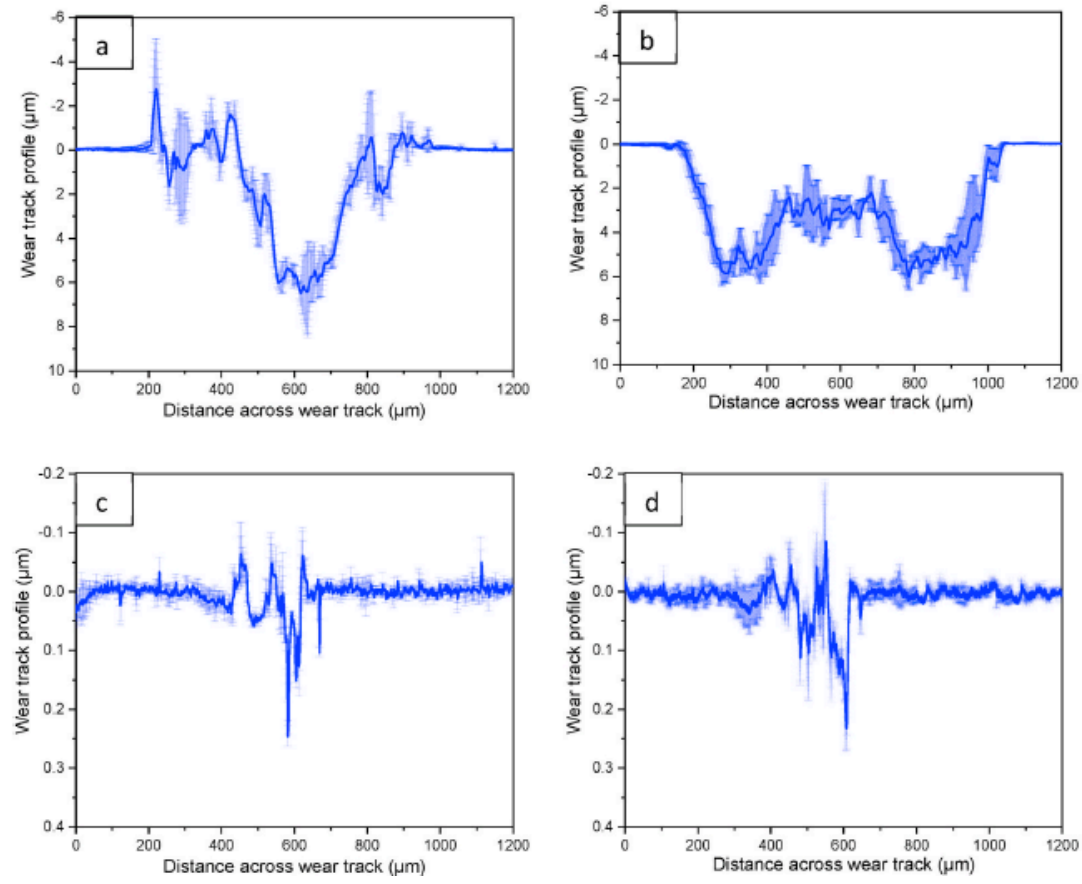
a
b
c
d
Wear track profile (μm)
Distance across wear track (μm)
0
200
400
600
800
1000
1200

Fig 9

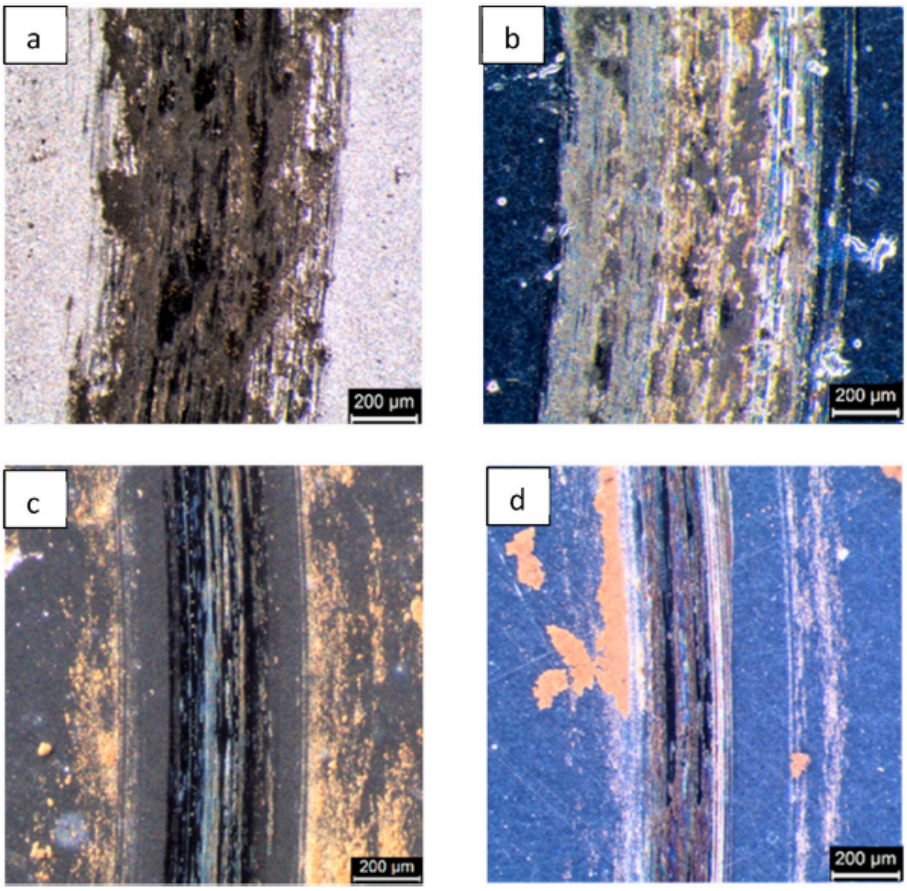
a
200 µm
b
200 µm
c
200 µm
d
200 µm

Fig 10

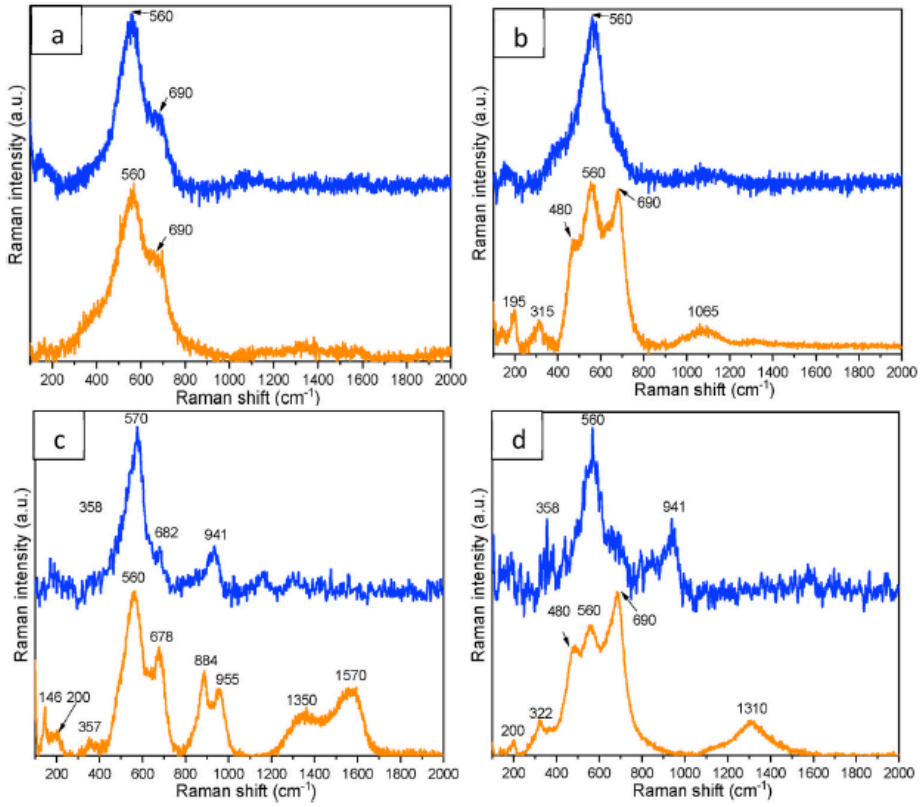
a
560
690
560
690
Raman intensity (a.u.)
200 400 600 800 1000 1200 1400 1600 1800 2000
Raman shift (cm-1)
b
560
560
690
480
195
315
1065
Raman intensity (a.u.)
200 400 600 800 1000 1200 1400 1600 1800 2000
Raman shift (cm-1)
c
570
358
682
941
560
678
884
955
1570
146 200
357
1350
Raman intensity (a.u.)
200 400 600 800 1000 1200 1400 1600 1800 2000
Raman shift (cm-1)
d
560
358
941
480 560
690
322
200
1310
Raman intensity (a.u.)
200 400 600 800 1000 1200 1400 1600 1800 2000
Raman shift (cm-1)

List of tables

Table 1:

grain size, roughness and impurities content.

	W (at.%)	Texture	d (nm)	R_a (nm)	Impurities					
					Fe (at.%)	Ar (at.%)	C (wt. ppm)	H (wt. ppm)	O (wt. ppm)	N (wt. ppm)
Ni-ED	0	200	750*	72 ± 4	–	–	5	1	25	–
Ni-PVD	0	111	47 ± 5	7 ± 2	0.13	0.10	–	–	–	–
NiW-ED	15	111	9 ± 1	12 ± 2	–	–	43	83	381	152
NiW-PVD	15	111	18 ± 2	13 ± 2	0.12	0.53	–	–	–	–

*done by TEM.

Tables 2:

Coatings	W (at. %)	R_d (µm)	P_d (µm)	Scratch width (µm)
Ni-ED	0	12	12	213 ± 7
Ni-PVD	0	13	19	155 ± 6
NiW-ED	15	1	9	134 ± 2
NiW-PVD	15	3	18	133 ± 2

Table 3:

Coatings	W (at. %)	H/E	Wear rate (mm^3/N.m)
Ni-ED	0	0.013	$1.8\ 10^{-4}$
Ni-PVD	0	0.023	$3.5\ 10^{-4}$
NiW-ED	15	0.038	$5.4\ 10^{-7}$
NiW-PVD	15	0.044	$1.0\ 10^{-6}$